LANGMUIR

Article

pubs.acs.org/Langmuir

Structure–Rheology Relationship in Nanosheet-Forming Peptoid Monolayers

Ellen J. Robertson, Eric Michael Nehls, and Ronald N. Zuckermann*

Molecular Foundry, Lawrence Berkeley National Laboratory, 1 Cyclotron Road, Berkeley, California 94720, United States

Supporting Information

ABSTRACT: Peptoid nanosheets are novel protein-mimetic materials that form from the supramolecular assembly of sequence-defined peptoid polymers. The component polymer chains organize themselves via a unique mechanism at the air–water interface, in which the collapse of a compressed peptoid monolayer results in free-floating, bilayer nanosheets. To impart functionality into these bilayer materials, structural engineering of the nanosheet-forming peptoid strand is necessary. We previously synthesized a series of peptoid analogues with modifications to the hydrophobic core in order to probe the nanosheet tolerance to different packing interactions. Although many substitutions were well-tolerated, routine surface pressure measurements and monolayer collapse isotherms were insufficient to explain which molecular processes contributed to the ability or inability of these peptoid analogues to form nanosheets. Here, we show that surface dilational rheology measurements of assembled peptoid monolayers at the air–water interface provide great insight into their nanosheet-forming ability. We find that a key property required for nanosheet formation is the ability to assemble into a solidlike monolayer in which the residence time of the peptoid within the monolayer is very long and does not exchange rapidly with the subphase. These collapse-competent monolayers typically have a characteristic time of diffusion-exchange values, τ_D, of >5000 s. Thus, rheological measurements provide an efficient method for assessing the nanosheet-forming ability of peptoid analogues. Results from these studies can be used to guide the rational design of peptoids for assembly into functional nanosheets.

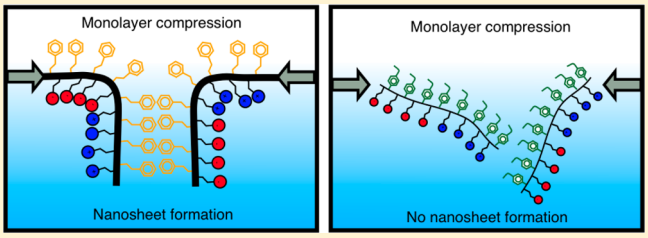

INTRODUCTION

The fabrication of functional, atomically defined two-dimensional (2D) nanomaterials is seeing increasing use in a growing number of applications.[1,2] In particular, polymer- and protein-based 2D nanomaterials can be engineered to serve as substrates for molecular recognition and catalysis, as membranes, and as templates for nanoparticle assembly and mineralization.[3−7] Peptoids[8,9] are protein mimetic polymers that hold much promise for assembly into 2D nanostructures for such applications. These sequence-defined polymers can be precisely designed to fold or assemble into a variety of structures.[10−16] One such structure is the recently discovered peptoid nanosheet, which is formed in water via a unique monolayer collapse mechanism at either the air–water or oil–water interface.[17] The method of creating 2D polymer nanostructures at the air–water interface has been extensively used, as it allows for the preorganization of amphiphilic species into defined structures.[3,18] In the nanosheet-forming mechanism, amphiphilic peptoids with a 2-fold periodic sequence pattern of ionic and hydrophobic monomers spontaneously adsorb to the interface in dilute aqueous solution to form a highly ordered monolayer intermediate. Upon compression of the surface, the monolayer buckles and collapses as a bilayer into the aqueous phase, with the hydrophobic groups forming an interior hydrophobic core and the ionic groups exposed on the solvent-exposed surface.

Recent efforts have focused on engineering the peptoid nanosheet structure to serve as a 2D molecular scaffold upon which to display diverse chemical functionality.[17] The introduction of new functionality into nanosheets requires making chemical modifications to either the hydrophilic monomers (for exterior functionalization) or the hydrophobic monomers (for interior functionalization) in the nanosheet-forming peptoid sequence. To better understand the degree to which the peptoid sequence can be modified without disrupting nanosheet formation, we examined a systematic series of analogues of our prototype sheet-forming peptoid sequence, $(Nae\text{-}Npe)_7\text{-}(Nce\text{-}Npe)_7$ (peptoid **1**).[19] For future applications, it is critical that these modifications do not disrupt the ability of the peptoids to efficiently form nanosheets.

Given the dependence of nanosheet formation on interfacial adsorption, one risk of introducing chemical modifications into the sequence is that they may significantly alter the hydrophobicity. A reduction in hydrophobicity could result in reduced interfacial adsorption, whereas an increase may result in unwanted aggregation. For example, certain peptoids with very hydrophilic loop insert sequences did not form a monolayer at the air–water interface.[17] This issue was overcome by replacing

Received: July 25, 2016
Revised: September 18, 2016

DOI: 10.1021/acs.langmuir.6b02736
Langmuir XXXX, XXX, XXX−XXX

half of the hydrophobic *N*-(2-phenylethyl)glycine monomers with *N*-(2-(4-biphenyl)ethyl)glycine, which served to increase the overall hydrophobicity of the peptoid so that it could again assemble into a monolayer capable of collapse into nanosheets.

Recent studies have shown, however, that the ability of a peptoid to form a monolayer is not the only requirement for nanosheet formation.[17] In one example, a negatively charged peptoid analog, $(Npe\text{-}Nce)_{14}$, was shown to adsorb to the oil–water interface, but surface vibrational spectroscopic studies revealed that charge–charge repulsions prevented these monolayers from collapsing into nanosheets. More recently, a study of peptoid structural analogues with varying hydrophobic groups revealed certain sequences that readily adsorbed to the air–water interface yet were unable to form nanosheets.[19] Thus, the ability to form a monolayer is clearly not sufficient to explain the nanosheet-formation ability. We therefore set out to study the rheological behavior of the monolayers described in ref 19 to better understand the primary factors impacting nanosheet formation.

In this work, we use interfacial dilational rheology to probe the physical properties of peptoid monolayers that directly impact their collapse into nanosheets. We compare a systematic set of peptoid analogues composed of differing hydrophobic monomers, whose nanosheet-making abilities were previously determined, to our standard nanosheet-forming peptoid **1**.[19] Interfacial dilational rheology is a powerful technique to probe the relationship between a monolayer's physical properties and the kinetic processes occurring within. Previous studies of polymer and protein monolayers using this technique have provided great insight into the monolayer solubility, viscoelasticity, and rates of relaxation processes[20−22] (such as surface–bulk diffusion exchange and molecular reorientation) occurring within the monolayer.[20−27] Here, surface dilational rheological measurements were used to complement Langmuir trough measurements, providing insight into the molecular-level processes that prevent certain peptoid monolayers from collapsing into nanosheets. Rheological studies are rapid and convenient, using small sample volumes (μL) so that screening for nanosheet-forming behavior can be rapidly performed. We demonstrate that a peptoid's rheological properties can be used to relate a small difference in the peptoid chemical structure to its ability to form a monolayer competent for collapse into a nanosheet bilayer. This information is essential to guide the design of engineered nanosheets with sophisticated functionality.

EXPERIMENTAL SECTION

Materials. Peptoids were synthesized and purified according to previously described protocols.[19] Peptoid stock solutions were prepared by dissolving pure, lyophilized powder into 2:1 DMSO/water (v/v) at a concentration of 2 mM. All buffers and solvents were obtained from commercially available sources and used without further purification.

Langmuir Trough Experiments. Surface pressure vs area isotherms were obtained using a Langmuir trough (KSV Nima mini trough) as previously described.[28] Briefly, a Teflon trough was thoroughly cleaned with ethanol and water obtained from a Milli-Q filtration system (18.2 MΩ cm^{-1}). The cleanliness of the trough was confirmed by measuring the neat air–water surface tension to be 72–73 mN/m with a paper Wilhelmy plate. After the removal of the water via aspiration, 10 mL of peptoid solution (20 μM in 10 mM Tris, pH 8) was added to the trough. Surface tension vs time measurements began once a clean interface was obtained by removing via aspiration the initial peptoid monolayer that formed while filling the trough. After the peptoid adsorbed to the air–water interface for 1800 s, surface area compression–expansion cycles began by reducing the surface area at a rate of 50 cm^2/min from 80 cm (open barriers) to 20 cm (closed barriers). Immediately after the barriers were closed, they were reopened at rate of 100 cm^2/min and then remained open for 900 s. After this 900 s wait time, the surface area compression–expansion cycle was repeated for at least five cycles. The surface tension was converted to surface pressure by subtracting the measured surface tension of the air–peptoid solution from the measured surface tension of the neat air–water interface (~72–73 mN/m). All surface pressure vs area isotherms shown are from the third compression–expansion cycles of single measurements. As shown in Figures S1 and S2, the shapes of the first few compression isotherms for each peptoid monolayer are similar. All measurements were repeated to confirm the peptoid interfacial behavior.

Surface Dilational Rheological Experiments. Surface dilational rheological properties of the peptoid monolayers were measured using the oscillating drop method[26,27,29] on a OneAttension Theta optical tensiometer (Biolin Scientific). Prior to measurements, all syringes, needles, and tubing were copiously washed with 70% ethanol and Milli-Q water (18.2 MΩ cm^{-1}) to ensure cleanliness, which was verified by a neat air–water interfacial tension value of ~72–73 mN/m. An 8–10 μL drop containing the peptoid solution (20 μM in 10 mM Tris, pH 8) was formed using a repeating drop dispenser. This drop was enclosed in a sealed cuvette to prevent evaporation over time. Images of the backlit drop were recorded with a Gigabit Ethernet camera (76 frames/s, 782 × 582 resolution) at 0.1 frame/s until the surface tension changed less than 1 mN/m in 600 s (~900–1200 s). The surface tension as a function of time was calculated using OneAttension software. Specifically, the drop shape was fit to the Laplace–Young equation to obtain the shape factor, β, which was then used in eq 1 to determine the surface tension, γ.

$$\gamma = \frac{\Delta\rho g b}{\beta} \tag{1}$$

Here, $\Delta\rho$ is the density difference between the two phases, g is the gravitational constant, and b is the radius at the drop apex. The reported surface pressure values at 900 s (SP_{900}) were obtained by averaging at least three measurements obtained using the pendant drop method and one measurement using the Wilhelmy plate method in the Langmuir trough, as discussed above.

After adsorption to the air–water interface, the surface dilational viscoelastic moduli of the peptoid monolayers on these drops were measured by monitoring the response of the surface tension (or surface dilational stress, γ) to a surface modification (or surface strain, A). Here, the surface modification was supplied by sinusoidally varying the surface area with a piezoelectric pump, as described by eq 2.

$$A = A^0 + \tilde{A}\sin(2\pi\omega t) \tag{2}$$

Here, A^0 is the initial surface area, $\tilde{A}$ is the amplitude of the area oscillations, ω is the frequency of the oscillation, and t is the time. $\tilde{A}$ was chosen to be relatively small (~4–5% of A^0) in an attempt to limit nonlinear surface responses.[27] In the linear response regime, the surface tension will respond according to eq 3.

$$\gamma = \gamma^0 + \tilde{\gamma}\sin(2\pi\omega t + \phi) \tag{3}$$

Here γ^0 is the initial surface tension, $\tilde{\gamma}$ is the amplitude of the surface tension response, and ϕ is the phase shift between the area oscillation and the surface tension response. These parameters were determined via OneAttension software and were then used to determine the surface dilational viscoelastic modulus E, as described by eq 4.

$$E = \frac{\tilde{\gamma}}{\tilde{A}/A^0}e^{i\phi} \tag{4}$$

E is a complex, frequency-dependent quantity in which the real part, E', is the surface dilational elasticity storage modulus and the imaginary part, E'', is the surface dilational loss modulus and is related to the surface dilatational viscosity κ, as given by eq 5.

$$E(\omega) = E' + E'' = E_0 + i2\pi\omega\kappa \tag{5}$$

In these experiments, E was measured for each peptoid monolayer at area oscillation frequencies ranging from 0.01 to 1 Hz. Each trace for E'

DOI: 10.1021/acs.langmuir.6b02736
Langmuir XXXX, XXX, XXX–XXX

and E'' shown is an average of at least three measurements, with the error bars representing ±1 standard deviation.

RESULTS AND DISCUSSION

Nanosheets are formed via a unique monolayer collapse mechanism at the air−water or oil−water interface.[17] Nano-

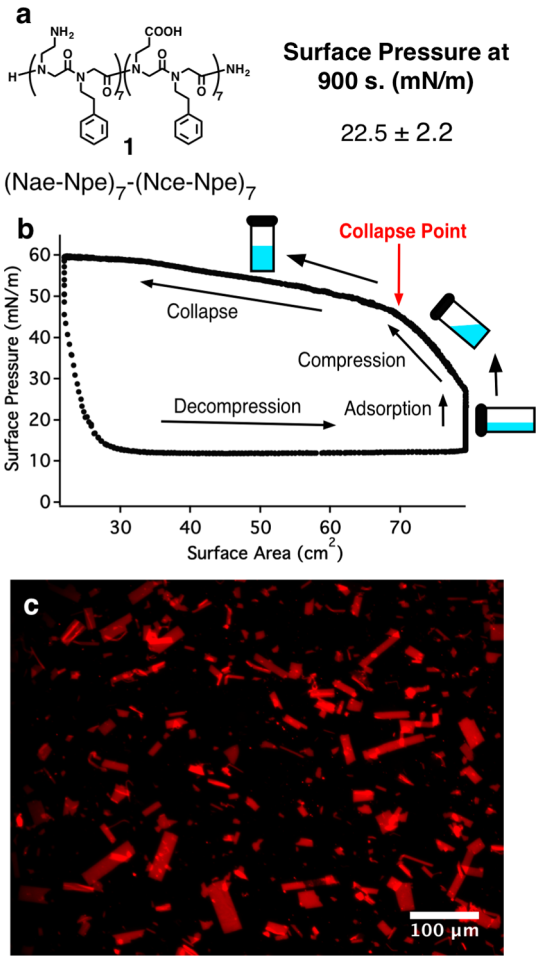

Figure 1. Surface behavior, monolayer collapse, and resulting nanosheets from the standard nanosheet-forming peptoid, $(Nae\text{-}Npe)_7\text{-}(Nce\text{-}Npe)_7$ (peptoid **1**). (a) Chemical structure and SP_{900} value for **1**. (b) Surface pressure vs surface area isotherm for **1** under the standard nanosheet-forming conditions (20 μM peptoid in 10 mM Tris buffer, pH 8), including a depiction of the vial rocking method. (c) Fluorescence microscopy images of nanosheets composed of **1** that have been incubated with 0.5 μM Nile red dye after the completion of nanosheet formation.

sheet-forming peptoids have been shown to spontaneously adsorb to the interface from aqueous solution within seconds, with continued adsorption occurring over time.[28] The standard nanosheet-forming peptoid that has been extensively used to make nanosheets is a 28-residue block-charge sequence, $(Nae\text{-}Npe)_7\text{-}(Nce\text{-}Npe)_7$[17] (Figure 1a, **1**), in which charged, polar *N*-(2-aminoethyl)glycine (Nae) and *N*-(2-carboxyethyl)glycine (Nce) monomers alternate with hydrophobic *N*-(2-phenylethyl)glycine (Npe) monomers. This amphiphilic peptoid dissolves in water at micromolar concentrations and readily adsorbs to the air−water interface, showing a surface pressure of 22.5 ± 2.2 mN/m after a wait time of 900 s (Figure 1a). We report the surface pressure value at 900 s (SP_{900}) as a metric for

Peptoid	Nanosheet Formation	SP_{900} (mN/m)
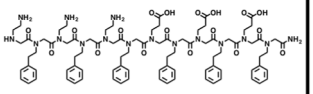 **2** $(Nae\text{-}Npe)_3\text{-}(Nce\text{-}Npe)_3$	No	14.8 ± 3.2
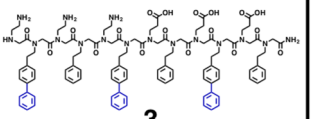 **3** Nae-Nbpe-Nae-Npe-Nae-Nbpe-Nce-Npe-Nce-Nbpe-Nce-Npe	Yes	26.2 ± 1.9
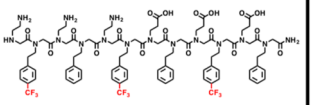 **4** Nae-Nfpe-Nae-Npe-Nae-Nfpe-Nce-Npe-Nce-Nfpe-Nce-Npe	Yes	32.9 ± 2.4

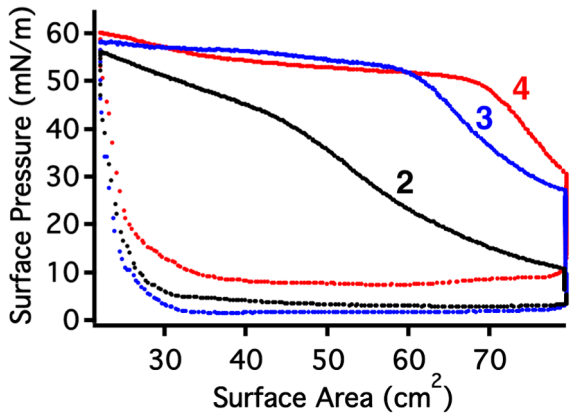

Figure 2. Chemical structures of the peptoids in the shortened chain series, including details of their respective nanosheet-forming ability, SP_{900} values, and Langmuir isotherms.

indicating the degree of interfacial adsorption under standard conditions (20 μM peptoid in 20 mM Tris at pH 8).[19] In this way, we can compare the extent of adsorption for the multiple peptoids used in this study. Although SP_{900} values are lower in magnitude than the true equilibrium surface pressure,[30] they serve as a conveniently measured standard for comparison.

Our previous studies have shown that peptoid adsorption and subsequent monolayer collapse can be monitored by surface pressure vs area measurements in a Langmuir trough.[17] To achieve this, peptoid is allowed to adsorb to the air−water interface with the paddles open for 900 s, during which time the surface pressure increases with monolayer formation as seen for peptoid **1** (Figure 1b). Subsequent closing of the paddles reduces the interfacial surface area, causing a rise in surface pressure, soon followed by an abrupt change in isotherm slope at the collapse point, which indicates that a peptoid monolayer is competent to collapse into nanosheets. During subsequent interface expansion, significant hysteresis appears in the isotherm as a result of material loss from the interface, which is consistent with the irreversible collapse of the monolayer in bilayer nanosheets. This

DOI: 10.1021/acs.langmuir.6b02736
Langmuir XXXX, XXX, XXX−XXX

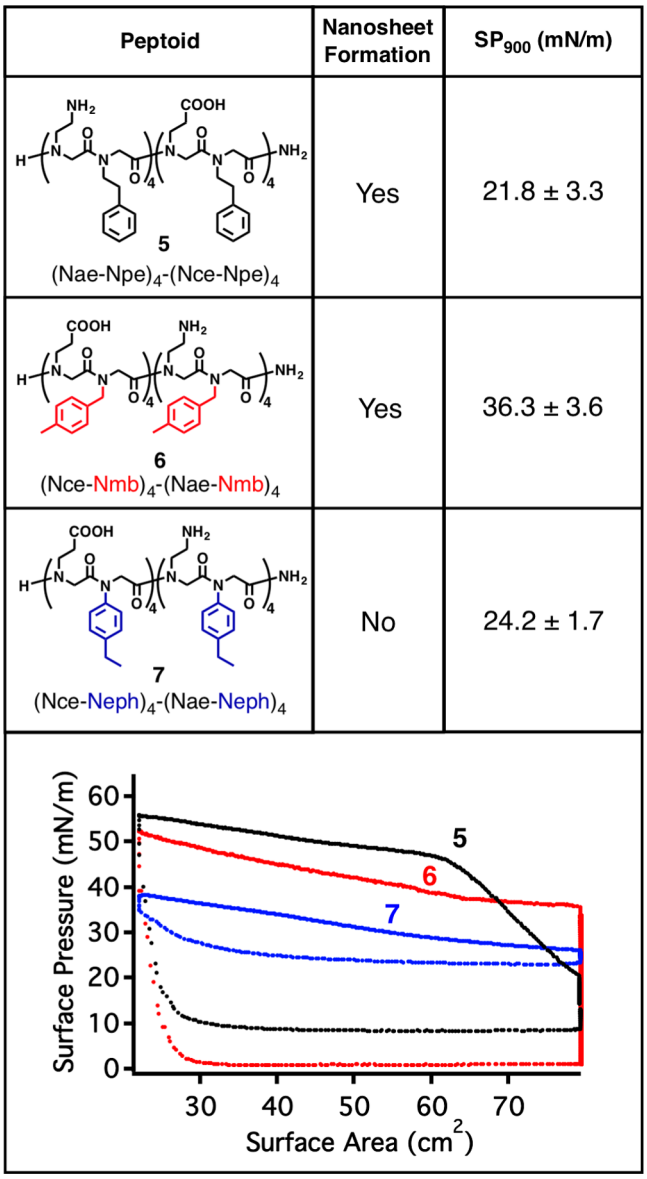

Figure 3. Chemical structures of the peptoids in the aromatic side chain length series, including details of their respective nanosheet-forming ability, SP_{900} values, and Langmuir isotherms.

process can be repeated multiple times, resulting in a conversion of 95% of the free peptoid into nanosheets.[28] Figure 1c shows resulting fluorescence microscopy images of peptoid nanosheets that have been stained with Nile red dye. For other peptoids, if a collapse point is not observed in the compression isotherm, then it generally indicates that nanosheets will not form. However, we show here that whereas these isotherms can indicate whether a certain peptoid will form nanosheets, they do not reveal the molecular-level details that either promote or hinder nanosheet formation.

A family of designed peptoid analogues was synthesized in an attempt to systematically probe the tolerance of substitutions within the hydrophobic core of the nanosheets. Peptoid modifications included adding various hydrophobic substituents to the phenylethyl group, changing the length of the side chain, replacing the aromatic group with aliphatic groups, and decreasing the main chain length. In-depth details concerning the design criteria for these peptoids and their nanosheet-forming capability via the vial rocking method have been reported elsewhere.[19] Here, we present the ability of these peptoid analogues to form a collapse-competent monolayer at the air−water interface and later describe the molecular-level details that prevent the nanosheet formation of certain peptoid monolayers.

Shortened Peptoid Sequences. Peptoids with only 12 residues were made in an effort to create stable nanosheets from the shortest possible sequence (Figure 2, peptoids **2**−**4**). In an earlier study, it was shown that the 16-residue analogue of peptoid **1** is the shortest known sequence to form nanosheets and that the 12mer with the hydrophobic Npe monomer ($(Nae\text{-}Npe)_3\text{-}(Nce\text{-}Npe)_3$, **2**) does not form nanosheets under the standard conditions.[37] Even though the SP_{900} of **2** reaches 14.8 ± 3.2 mN/m, suggesting that a monolayer forms, a distinct collapse point is not observed in its compression isotherm (Figure 2). Instead, the slope of the surface-pressure response remains nearly constant during monolayer compression. Upon area expansion, hysteresis is present but to a lesser extent than seen in the isotherm of the nanosheet-forming peptoids. This hysteresis indicates that material is still lost from the surface but not because of the formation of peptoid nanosheets. Instead, compression may force free peptoid or aggregates from the surface. To potentially increase the strength of peptoid packing interactions within the monolayer, an increase in the hydrophobicity of the 12mer peptoid was accomplished by incorporating either *N*-2-((4-biphenyl)ethyl)glycine (Nbpe) or *N*-2-(4-(trifluoromethyl)-phenylethyl)glycine (Nfpe) monomers into the peptoid (Figure 2, peptoids **3** and **4**). These modifications to the hydrophobic monomers of **2** were successful, with both peptoids **3** and **4** producing nanosheets. It is likely that the increased surface activity of **3** (SP_{900} 26.2 ± 1.9 mN/m) and **4** (SP_{900} 32.9 ± 2.4 mN/m) relative to that of **2** results in monolayers capable of collapse, as indicated in the isotherms of **3** and **4** (Figure 2).

Aromatic Side Chain Length. In a series of 16mer analogues (Figure 3, peptoids **5**−**7**), the position of the aromatic ring was varied with respect to the peptoid backbone. This positioning strongly affected the ability to form nanosheets. With the standard Npe hydrophobic monomer, in which the aromatic ring is two carbons away from the backbone, nanosheets readily form from **5** under the standard conditions in a rocking vial. Accordingly, this peptoid assembles at the air−water interface, with an SP_{900} of 21.8 ± 3.3 mN/m. Moreover, a collapse point is observed in its isotherm (Figure 3), the shape of which resembles that of **1**. It is likely that the isotherms of **1** and **5** look similar because these peptoids have the same hydrophobic monomer (Npe) and therefore may pack similarly at the air−water interface. Peptoids in which the *N*-(4-methylbenzyl)glycine (Nmb) monomer is incorporated (**6**) are still capable of forming nanosheets even though the aromatic ring is located one carbon closer to the peptoid backbone. Here, the surface activity of **6** (SP_{900} 36.3 ± 3.6 mN/m) significantly increases relative to that of **5**, with the collapse point appearing abruptly upon monolayer compression (Figure 3). Because this collapse point is difficult to see clearly because of its abruptness, we confirm its occurrence by obtaining the surface pressure vs area isotherm of the peptoid **6** monolayer after an adsorption time of only 450 s (Figure S3). When the aromatic ring is directly attached to the backbone, as with the *N*-(4-ethylphenyl)glycine (Neph) monomer (**7**), nanosheets are no longer able to form. Even though the surface activity of **7** (SP_{900} 24.2 ± 1.7 mN/m) is greater than that of **5**, a collapse point is not observed in its isotherm (Figure 3). Here, the lack of a collapse point does not reveal the molecular-level

DOI: 10.1021/acs.langmuir.6b02736
Langmuir XXXX, XXX, XXX−XXX

Peptoid	Nanosheet Formation	SP_{900} (mN/m)	Peptoid	Nanosheet Formation	SP_{900} (mN/m)
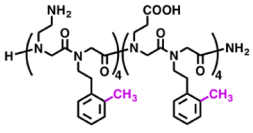 **8** (Nae-N2mpe)$_4$-(Nce-N2mpe)$_4$	No	28.1 ± 1.3	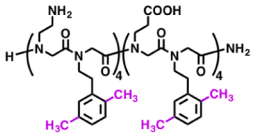 **11** (Nae-N25dmpe)$_4$-(Nce-N25dmpe)$_4$	No	32.1 ± 2.0
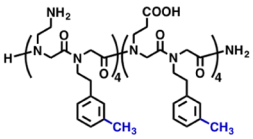 **9** (Nae-N3mpe)$_4$-(Nce-N3mpe)$_4$	Yes	32.1 ± 2.5	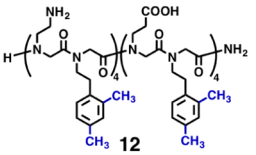 **12** (Nae-N24dmpe)$_4$-(Nce-N24dmpe)$_4$	Yes*	32.4 ± 2.6
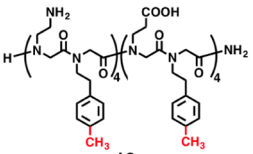 **10** (Nae-N4mpe)$_4$-(Nce-N4mpe)$_4$	Yes	34.6 ± 1.0	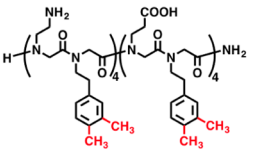 **13** (Nae-N34dmpe)$_4$-(Nce-N34dmpe)$_4$	Yes	37.4 ± 1.4

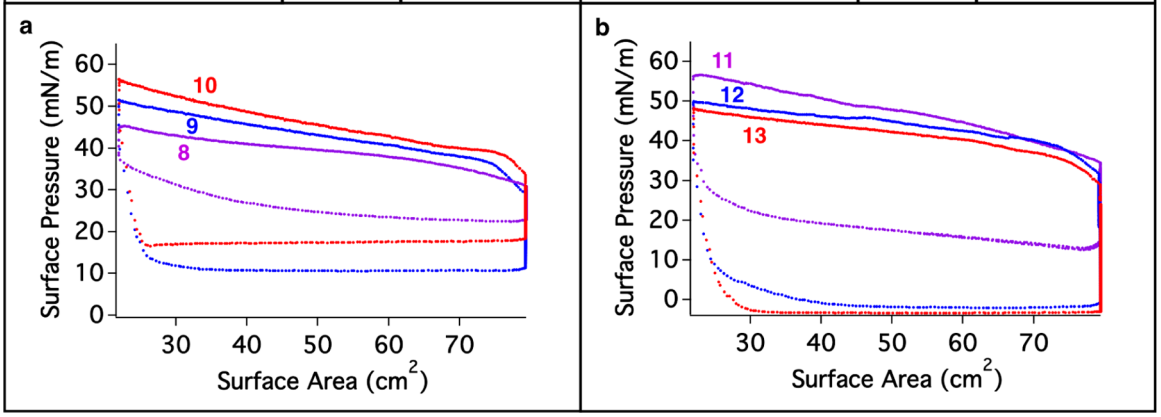

Figure 4. Chemical structures of the peptoids in the aromatic ring substituent series, including details of their respective nanosheet-forming ability, SP_{900} values, and Langmuir isotherms of the (a) monomethyl-substituted and (b) dimethyl-substituted analogues.

factors that prevent an assembled monolayer from forming nanosheets.

Aromatic Ring Substituents. Next, we explored the addition of substituents to the aromatic ring of the Npe monomer that could be tolerated in nanosheet formation. We synthesized a series of peptoids in which the aromatic group was either monomethyl substituted (**8**–**10**) or dimethyl substituted (**11**–**13**) (Figure 4). For these peptoids, monolayer collapse and therefore nanosheet formation depended upon the positioning of the methyl substituent. For peptoid **8**, which was synthesized with *N*-2-(2-(methyl)phenylethyl)glycine (N2mpe) monomers, nanosheets did not form despite monolayer formation (SP_{900} 28.1 ± 1.3 mN/m). Accordingly, no collapse point was observed in the isotherm of **8** (Figure 4a). Nanosheet formation was recovered when either *N*-2-(3-(methyl)phenylethyl)glycine (N3mpe) or *N*-2-(4-(methyl)phenylethyl)glycine (N4mpe) monomers were incorporated to give peptoid **9** or **10**. As expected, the isotherms of **9** and **10** both show collapse points (Figure 4a). Thus, the substitution of the aromatic ring at the meta and para positions is well tolerated, but substitution at the ortho position is not.

Even though substitution at the ortho position was not tolerated in nanosheet formation, a second methyl substituent was added to **8** in an attempt to recover monolayer collapse and nanosheet formation. For the peptoid with *N*-2-(2,5-(dimethyl)-phenylethyl)glycine (N25dmpe) monomers (**11**), neither monolayer collapse (Figure 4b) nor nanosheet formation was recovered, despite an increase in the SP_{900} (32.1 ± 2.0 mN/m) relative to that of **8**. Monolayer collapse (Figure 4b) and nanosheet formation, however, were recovered when the peptoid contained *N*-2-(2,4-(dimethyl)phenylethyl)glycine (N24dmpe) monomers (**12**). As shown previously, however, nanosheets made from **12** were unstable in solution over time. Stable nanosheets formed from peptoids with *N*-2-(3,4-(dimethyl)-phenylethyl)glycine (N34dmpe) monomers (**13**), which lacks an ortho substituent. As expected, this peptoid very readily adsorbed to the air–water interface (SP_{900} 37.4 ± 1.4 mN/m) and showed a collapse point in its isotherm (Figure 4b). As with the monosubstituted analogues, substitution at the ortho position is not tolerated in stable nanosheets.

Aliphatic Core Nanosheets. A series of peptoids were prepared where the aryl residues of **1** were replaced with aliphatic

DOI: 10.1021/acs.langmuir.6b02736
Langmuir XXXX, XXX, XXX–XXX

Peptoid	Nanosheet Formation	SP_{900} (mN/m)
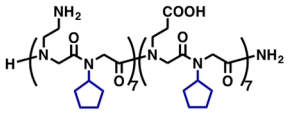 **14** (Nae-Ncp)$_7$-(Nce-Ncp)$_7$	No	13.3 ± 4.6
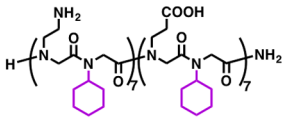 **15** (Nae-Nch)$_7$-(Nce-Nch)$_7$	No	23.8 ± 3.1
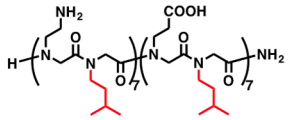 **16** (Nae-Nmbu)$_7$-(Nce-Nmbu)$_7$	Yes	36.9 ± 1.4

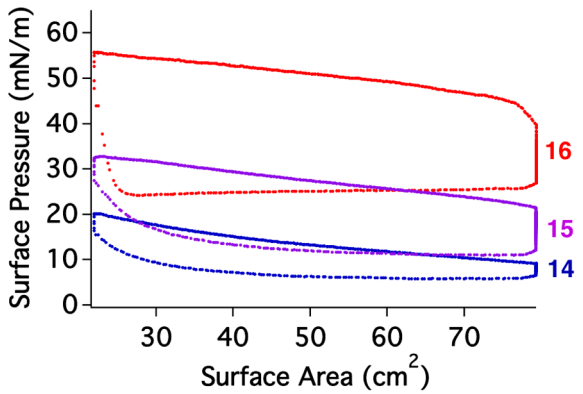

Figure 5. Chemical structures of the peptoids in the aliphatic core series, including details of their respective nanosheet-forming ability, SP_{900} values, and Langmuir isotherms.

monomers (Figure 5, peptoids **14**–**16**) in order to determine if an aromatic core is a key requirement for nanosheets. We chose two cyclic side chains as well as leucine-like analogue *N*-(3-methylbutyl)glycine (Nmbu) because its side chain is branched and is known to pack with itself in leucine zipper proteins. The peptoid with hydrophobic *N*-cyclopentylglycine (Ncp) monomers (**14**) was unable to form a monolayer capable of collapse into nanosheets (Figure 5). This may be due to an inability to form a dense enough monolayer at the air–water interface, as indicated by a relatively low SP_{900} (Figure 5, 13.3 ± 4.6 mN/m). Even though incorporating *N*-cyclohexylglycine (Nch) monomers into the peptoid increased the surface activity of peptoid **15** (Figure 5, SP_{900} 23.8 ± 3.1 mN/m) relative to that of **14**, **15** was also unable to form a monolayer capable of collapse into nanosheets (Figure 5). Only peptoid **16** was capable of producing nanosheets showing both a strong propensity for surface adsorption (SP_{900} 36.14 ± 1.4 mN/m) and the formation of a collapsible monolayer (Figure 5).

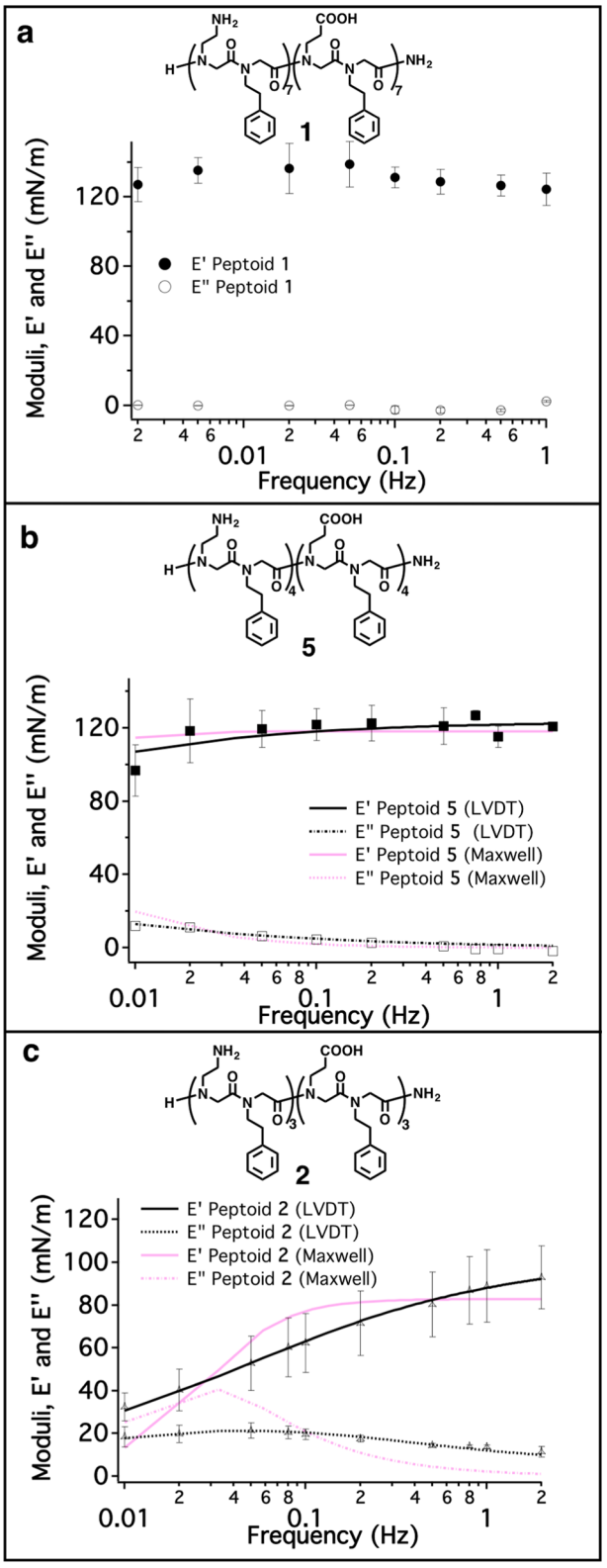

Figure 6. Surface dilational rheological data for the monolayers composed of peptoids **1**, **5** ,and **2** in the (Nae-Npe)$_n$-(Nce-Npe)$_n$ chain length series, showing E' (solid symbols) and E'' (open symbols) as a function of the frequency of the sinusoidal area perturbation. Rheological data for the 28-residue (peptoid **1**) monolayer (a), the 16-residue (peptoid **5**) monolayer (b), and the 12-residue (peptoid **2**) monolayer (c). For the peptoid **2** and **3** monolayers, the data were globally fit to both the LVDT (black traces) and Maxwell (pink traces) models.

DOI: 10.1021/acs.langmuir.6b02736
Langmuir XXXX, XXX, XXX–XXX

Table 1. Parameters Obtained from the Npe Main Chain Length Series Rheological Data[a]

peptoid	model	E_0 (mN/m)	τ_D (s)	κ (mNs/m)	χ^2
$(Nae\text{-}Npe)_7$-$(Nce\text{-}Npe)_7$ (**1**)	N/A	131 ± 5	∼∞	N/A	N/A
$(Nae\text{-}Npe)_4$-$(Nce\text{-}Npe)_4$ (**5**)	LVDT	123 ± 1	5000 ± 2000	0.6 ± 0.2	370
$(Nae\text{-}Npe)_4$-$(Nce\text{-}Npe)_4$ (**5**)	Maxwell	118 ± 2	600 ± 100	N/A	657
$(Nae\text{-}Npe)_3$-$(Nce\text{-}Npe)_3$ (**2**)	LVDT	103.1 ± 0.6	44 ± 1	∼0	37
$(Nae\text{-}Npe)_3$-$(Nce\text{-}Npe)_3$ (**2**)	Maxwell	84 ± 4	37 ± 6	N/A	3811

[a]The data for peptoids **2** and **5** were globally fit to both the LVDT (eqs 6 and 7) and Maxwell (eqs 8 and 9) models using a nonlinear least-squares fitting routine. For peptoid **1**, ∼∞ indicates that the residence time of the peptoid within the monolayer is longer than can be measured with the experiment, so these data were not fit. Here, E_0 is given as the average E' value for all area oscillation frequencies measured. The χ^2 values are metrics for how well the data fit the model, with smaller values indicating a better fit.

From the surface pressure vs area isotherms alone, it is unclear as to what occurs on the molecular level to either promote or inhibit monolayer collapse and nanosheet formation. In some cases, the degree of adsorption can play a significant role, as reflected by the SP_{900} values. For instance, the SP_{900} values for **2** and **14** were significantly lower than for standard nanosheet-forming peptoid **1**, and no nanosheets were observed. Interestingly, however, all other peptoid analogs that did not form nanosheets had SP_{900} values equal to or greater than **1**, indicating that interfacial adsorption is not the only process that can limit nanosheet formation. Instead, other factors related to monolayer assembly, such as the degree of monolayer fluidity and interactions between adsorbed peptoid chains, must contribute to the inability of some peptoid analogues to form nanosheets.

Surface Dilational Rheology. To probe the factors that prevent a peptoid monolayer from collapsing into bilayers, we measured the physical properties of the monolayers using surface dilational rheology. This technique provides information such as the degree of monolayer dilational elasticity and viscosity. Moreover, this technique can shed light on the kinetic processes that occur in monolayers by providing time scales for events such as the diffusion exchange between bulk and surface-adsorbed species, molecular reorientation, and chemical reactions.[27,29,31−33] Specifically, the characteristic frequency of a surface relaxation event can be determined by plotting E' and E'' as a function of the frequency of the surface area oscillation. Subsequently, these data can be fit to a model corresponding to a specific relaxation event. Two common models to fit surface dilational rheological data are the Lucassen−van den Temple (LVDT) expression,[20,23,29,33−35] which describes the diffusion-controlled exchange between soluble surface and bulk species, and the Maxwell expression,[20,21,23] which describes a single relaxation event that occurs within an insoluble monolayer. The LVDT model is given by eqs 6 and 7.

$$E' = E_0 \frac{1 + \Omega}{1 + 2\Omega + 2\Omega^2} \tag{6}$$

$$E'' = E_0 \frac{\Omega}{1 + 2\Omega + 2\Omega^2} + \kappa\omega \tag{7}$$

Here, $\Omega = (\tau_D\omega)^{-1/2}$, where $\tau_D = 1/\omega_D$ is the characteristic time of diffusion exchange, ω_D is the corresponding characteristic frequency, and E_0 ($\omega \to \infty$) is the Gibbs elasticity for soluble surface species.[20,23,29,32,36] Here, the τ_D value can be thought of as the residence time of the peptoid in the monolayer, with larger τ_D values corresponding to longer times taken by the peptoid to desorb or readsorb to the interface upon compression or expansion. The term $\kappa\omega$ is added to E'' to account for behavior at high frequencies in which the insoluble nature of the monolayer can lead to viscous dissipation.[23]

The Maxwell expression is the simplest case of the generalized linear viscoelastic model, with only one relaxation mode, and is given by eqs 8 and 9:

$$E' = E_M \frac{\tau_M{}^2\omega^2}{1 + \tau_M{}^2\omega^2} \tag{8}$$

$$E'' = E_M \frac{\tau_M\omega}{1 + \tau_M{}^2\omega^2} \tag{9}$$

Here, $\tau_M{}^2$ is the characteristic relaxation time (with corresponding frequency ω_M) and E_M is the modulus as $\omega \to \infty$. In both the LVDT and Maxwell models, E' and E'' are 0 mN/m when $\omega \ll \omega_D$ and $\omega \ll \omega_M$, respectively. In this regime, monolayers are fluidlike. A peak in E'' appears when $\omega = \omega_D$ and $\omega = \omega_M$ and corresponds to the time scale of the surface-bulk diffusion exchange and surface relaxation event, respectively. When $\omega \gg \omega_D$ and $\omega \gg \omega_M$, the monolayer is solidlike because the surface molecules do not have sufficient time to either exchange with molecules in the bulk or relax at the surface.

Distinct differences occur in the surface dilational rheological behavior of the peptoid monolayers that form nanosheets compared to those that do not, which can clearly be observed in the data for the $(Nae\text{-}Npe)_n$-$(Nce\text{-}Npe)_n$ peptoid length series (Figure 6a−c). For **1** (Figure 6a), E' and E'' do not significantly change as a function of the frequencies probed, with E'' remaining close to 0 mN/m for all frequencies. This behavior indicates that the **1** monolayer exhibits no relaxation events occurring on the time scale of the experiment. For **5** (Figure 6b) and **2** (Figure 6c), E' decreases with decreasing frequency and E'' is no longer constant and close to 0 mN/m. This behavior indicates that relaxation events occur in the **2** and **5** monolayers on a time scale that can be accessed with these experiments.

To determine the specific nature of the relaxation events occurring in the **2** and **5** monolayers, the moduli vs frequency data were fit to both the modified LVDT (eqs 6 and 7) and Maxwell (eqs 8 and 9) models. Here, E' and E'' were simultaneously fit using a global routine to provide greater confidence in the fit parameters. The resulting fit parameter and associated errors are listed in Table 1. Here, the χ^2 value is a metric for how well the models fit the data, with smaller χ^2 values indicating a better fit. For both **2** and **5**, the χ^2 values are smaller when the data are fit to the LVDT equations than when the data are fit to the Maxwell equations. This indicates that the LVDT model is a better description of the data and that the relaxation event is the diffusion exchange between surface and bulk species rather than a relaxation event (such as molecular reorientation or lateral diffusion) occurring within an insoluble monolayer. Such lateral relaxation events may be occurring, but their contribution

DOI: 10.1021/acs.langmuir.6b02736
Langmuir XXXX, XXX, XXX−XXX

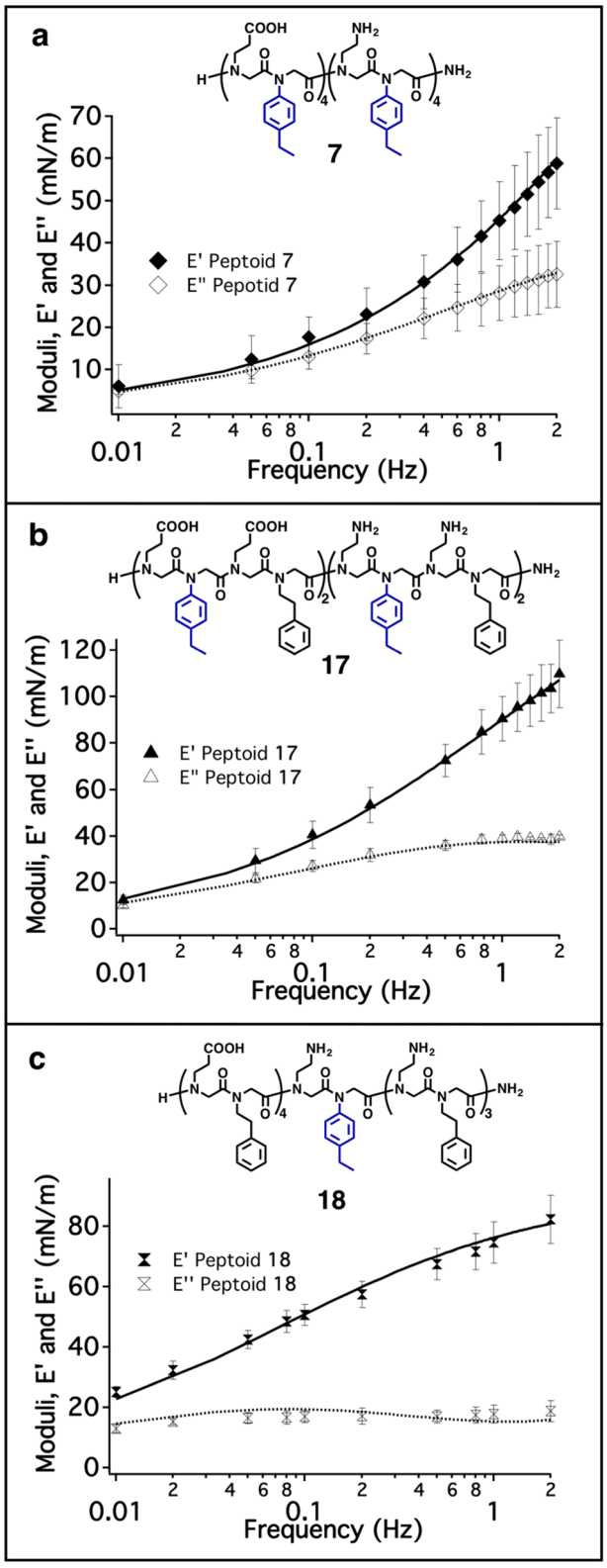

Figure 7. Surface dilational rheological data for the monolayers composed of 16-residue peptoids containing the N-aryl Neph monomer, showing E' (solid symbols) and E'' (open symbols) as functions of the frequency of the sinusoidal area perturbation. Rheological data for (a) the $(Nce\text{-}Neph)_4\text{-}(Nae\text{-}Neph)_4$ (**7**) monolayer, (b) the $(Nce\text{-}Neph\text{-}Nce\text{-}Npe)_2\text{-}(Nae\text{-}Neph\text{-}Nce\text{-}Npe)_2$ (**17**) monolayer, and (c) the $(Nce\text{-}Npe)_4\text{-}Nae\text{-}Neph\text{-}(Nae\text{-}Npe)_3$ (**18**) monolayer. All E' (solid lines) and E'' (dotted lines) data were globally fit to the LVDT model.

is small enough that they cannot be ascertained from the fits to the data. All subsequent moduli vs frequency data were fit to the LVDT model, which was shown to represent the data better than did the Maxwell model for all peptoid monolayers discussed in this article.

Previous studies have shown that a decrease in the length of standard nanosheet-forming peptoid **1** results in a decrease in the stability of the peptoid nanosheet, with 16-residue peptoid **5** being the shortest peptoid able to form stable nanosheets.[37] The degree of monolayer fluidity follows this trend, as assessed by the characteristic residence time of the peptoid in the monolayer (τ_D, Table 1). Here, the longest τ_D is seen for the **1** monolayer ($\sim\infty$ s, i.e., longer than the time scale of the experiment), and the shortest τ_D is seen for the **2** monolayer (44 ± 1 s). The τ_D value for the monolayer of **5** (5000 ± 2000 s) is relatively long compared to the τ_D for the monolayer of **2**. The long τ_D values for **1** and **5** indicate that the individual peptoid strands in these monolayers do not rapidly exchange with peptoids in bulk solution. This property points to interchain interactions that are strong enough to form solidlike monolayers that are capable of collapse into nanosheets. Compared to **1** and **5**, the shorter τ_D value for **2** indicates that individual peptoid strands in this monolayer more readily exchange with peptoids in bulk solution. Here, weaker interchain interactions lead to a more fluidlike monolayer that is unable to collapse into nanosheets. This result is consistent with atomic simulations of peptoid nanosheets, which showed that nanosheets composed of peptoids with 12 residues possess a high density of pores.[37] These pores exist because of unfavorable interactions at chain−chain termini, thereby limiting the degree to which the peptoids can pack together.

Another measure that was anticipated to be related to monolayer stability and possibly correlated with monolayer collapse behavior is the Gibbs elasticity, E_0.[20,23,29,32,36] This is the elasticity of a monolayer as the frequency of surface area oscillation approaches infinity. At high area oscillation frequencies, the monolayer will behave as a solidlike rheological body because there is not sufficient time for diffusion exchange to occur. This metric has been extensively applied as a measure of monolayer stability.[36] Within this peptoid main chain length series, there appears to be a trend, with higher values of E_0 corresponding to slower diffusion-exchange rates and improved sheet-forming behavior. However, this trend was not consistent within other series or between series. As such, the Gibbs elasticity will not be discussed in further detail, though a table with all of the fit parameters can be found in the Supporting Information (Table S1).

Diffusion Exchange Rates. The characteristic residence time of the peptoid within the monolayer (τ_D), in addition to providing valuable information about the molecular events taking place at the interface, proved to be predictive of the collapse competency of all peptoid sequences tested. Results from the surface dilational rheology studies reveal molecular-level details that prevent well-formed monolayers from collapsing into nanosheets. We report results from select peptoids to demonstrate the effect of peptoid monolayer fluidity on the ability to form peptoid nanosheets.

As discussed above (Figure 3), it is interesting that peptoid **7** readily assembles at the air−water interface yet does not form nanosheets, which suggests that factors other than peptoid hydrophobicity and monolayer formation play a role in the interchain packing at the interface. As with **2**, the data from **7** shows that E' increases with increasing frequency and E'' is

DOI: 10.1021/acs.langmuir.6b02736
Langmuir XXXX, XXX, XXX−XXX

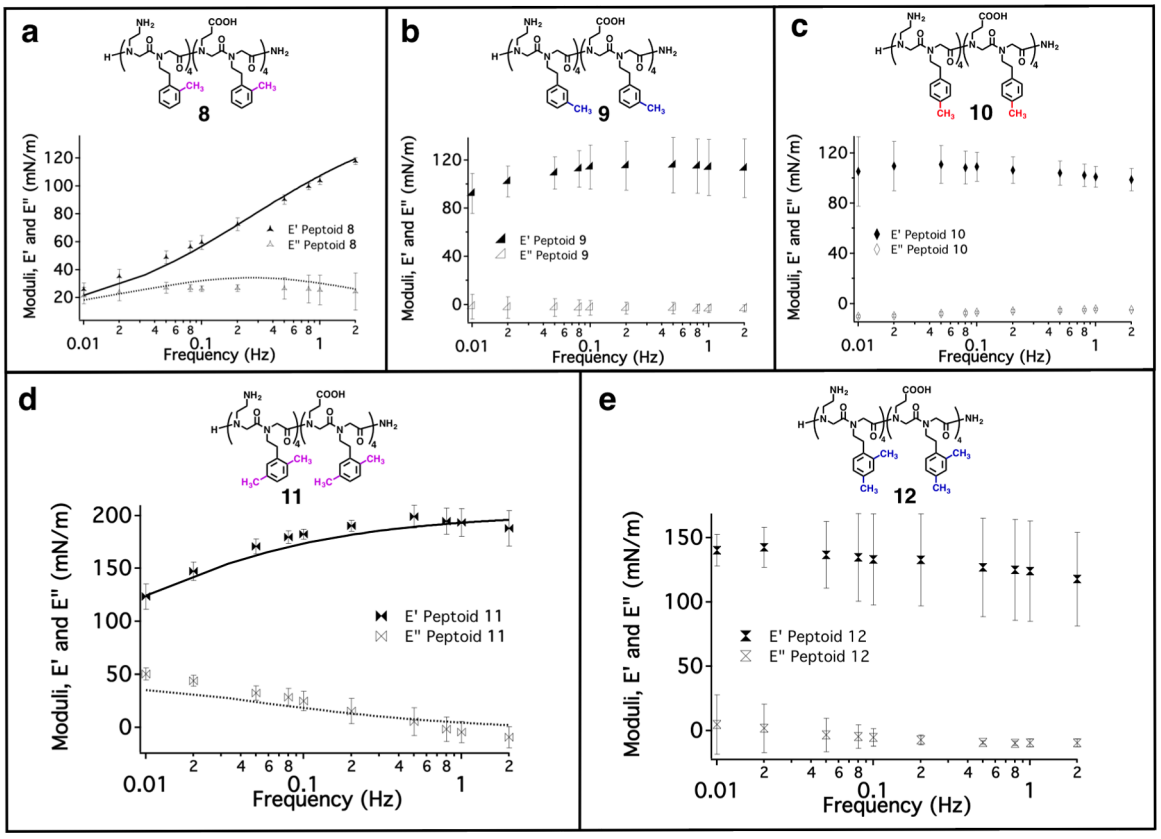

Figure 8. Surface dilational rheological data for the monolayers composed of 16-residue peptoids in which all Npe monomers are either monomethyl- or dimethyl-substituted, showing E' (solid symbols) and E'' (open symbols) as a function of the frequency of the sinusoidal area perturbation. Rheological data for (a) the $(Nae\text{-}N2mpe)_4$-$(Nce\text{-}N2mpe)_4$ (**8**) monolayer, (b) the $(Nae\text{-}N3mpe)_4$-$(Nce\text{-}N3mpe)_4$ (**9**) monolayer, (c) the $(Nae\text{-}N4mpe)_4$-$(Nce\text{-}N4mpe)_4$ (**10**) monolayer, (d) the $(Nae\text{-}N25dmpe)_4$-$(Nce\text{-}N25dmpe)_4$ (**11**) monolayer, and (e) the $(Nae\text{-}N24dmpe)_4$-$(Nce\text{-}N24dmpe)_4$ (**12**) monolayer. The E' (solid lines) and E'' (dotted lines) data were globally fit to the LVDT model for the **8** and **11** monolayers.

nonzero (Figure 7a). The fit to this data shows that the residence time for the peptoid with the monolayer is very short, with a τ_D value of 0.40 ± 0.02 s, and that the monolayer is fluidlike. As described recently,[19] the design behind peptoid **7** was to induce the peptoid into an all-trans configuration[15] in order to favor the extended, Σ strand secondary structure[37] that is thought to be adopted by peptoids within stable nanosheets.

To further investigate the tolerance of a peptoid sequence to N-aryl residue substitutions, we decreased the number of Neph monomers per peptoid chain. Specifically, peptoid **17** [$(Nce\text{-}Neph\text{-}Nce\text{-}Npe)_2$-$(Nae\text{-}Neph\text{-}Nae\text{-}Npe)_2$] was synthesized such that every other Neph monomer in **7** was replaced with an Npe monomer (Figure 7b, peptoid **17**). For this peptoid monolayer, the rheological data still show a rapid exchange between peptoids at the air−water interface and peptoids in bulk solution. Here, the τ_D value (2.4 ± 0.1 s) is only 1 order of magnitude greater than that seen for the Neph monolayer. Even for the monolayer composed of $(Nce\text{-}Npe)_4$-Nae-Neph-$(Nae\text{-}Npe)_3$ (Figure 4c, peptoid **18**) in which all but one monomer in the peptoid sequence is replaced with the Npe monomer, peptoid desorption and readsorption still occur within the time scale of the experiment as the surface area is changed, albeit with a longer peptoid residence time in the monolayer (τ_D = 28 ± 2 s) than seen in the monolayers of either **7** or **17**. Overall, decreasing the number of Neph monomers within the peptoid increases the peptoid residence time in the monolayer, likely by increasing the degree of intermolecular interactions between hydrophobic groups of neighboring chains within the monolayer. However, having only one Neph monomer in the middle of the peptoid strand was still enough to disrupt the network of interchain interactions required from a solidlike monolayer that is capable of collapse into nanosheets. Previous studies of *N*-aryl peptoids have shown that when phenyl groups are directly attached to the nitrogen of the peptoid backbone, the rings lay in the plane that is perpendicular to the plane of the peptoid backbone, decreasing the peptoid conformational flexibility.[15] These factors may combine to inhibit $\pi-\pi$ stacking between aromatic rings on neighboring peptoid strands within the monolayer, thereby allowing peptoid desorption and readsorption to rapidly occur as the surface area is changed.

Although 16-residue peptoids containing even one *N*-aryl residue in the middle of the peptoid chain cannot form nanosheets, the rheological studies suggest that *N*-aryl residues may be tolerated in nanosheet formation if the number of Npe monomers per chain is further increased. This could occur by increasing the length of the peptoid chain to 28 residues so that longer blocks of Npe monomers are present to promote intermolecular interactions within the monolayer that slow diffusion exchange.

The disruption of interchain interactions within the peptoid monolayer is also observed in the rheological data of the series of peptoids with monomethyl-substituted phenylethyl groups (Figure 8a−c). Here, the disruption depends upon the position of the methyl group(s) on the aromatic ring. For the $(Nae\text{-}N2mpe)_4$-$(Nce\text{-}N2mpe)_4$ monolayer (**8**, Figure 8a), which does not collapse to form nanosheets, the small τ_D value (7.6 ± 0.9 s)

DOI: 10.1021/acs.langmuir.6b02736
Langmuir XXXX, XXX, XXX−XXX

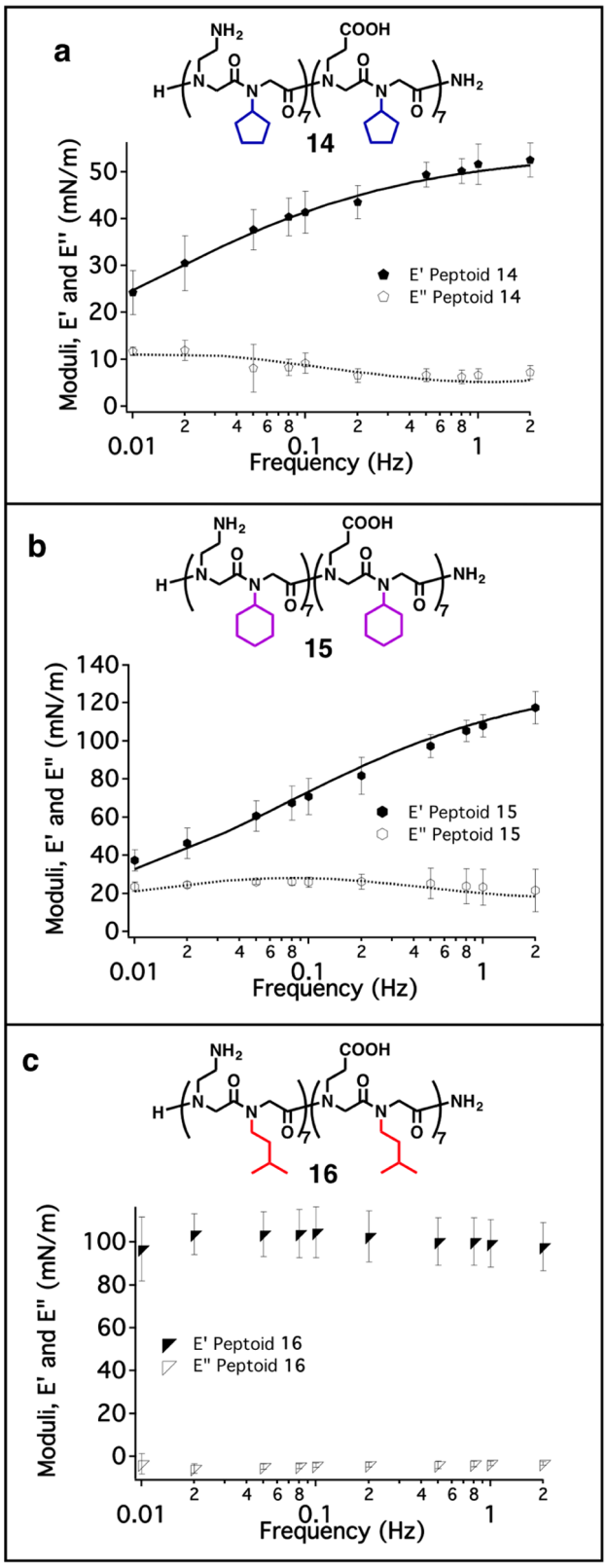

Figure 9. Surface dilational rheological data for the monolayers composed of 28-residue peptoids with aliphatic hydrophobic monomers, showing E' (solid symbols) and E'' (open symbols) as a function of the frequency of the sinusoidal area perturbation. Rheological data for (a) the $(Nae\text{-}Ncp)_4$-$(Nce\text{-}Ncp)_4$ (**14**) monolayer, (b) the $(Nae\text{-}Nch)_4$-$(Nce\text{-}Nch)_4$ (**15**) monolayer, and (c) the $(Nae\text{-}Nmbu)_4$-$(Nce\text{-}Nmbu)_4$ (**16**) monolayer. The E' (solid lines) and E'' (dotted lines) data were globally fit to the LVDT model for the **14** and **15** monolayers.

again indicates a fluidlike monolayer with relatively weak interstrand interactions that allow for a short peptoid residence time within the monolayer. For the $(Nae\text{-}N3mpe)_4$-$(Nce\text{-}N3mpe)_4$ (**9**, Figure 8b) and $(Nae\text{-}N4mpe)_4$-$(Nce\text{-}N4mpe)_4$ (**10**, Figure 8c) monolayers, both of which collapse to form nanosheets, the rheological data show the absence of peptoid desorption and readsorption occurring on a time scale that can be accessed by the experiment. Again, we observe that peptoid monolayers capable of collapse into nanosheets are solidlike.

The monolayer residence time for peptoids in which the ortho position of the Npe monomer is methyl-substituted increased when a second methyl substituent was added to the aromatic ring in either the meta or para position (Figure 8d,e). Specifically, the τ_D value of the $(Nae\text{-}N4mpe)_4$-$(Nce\text{-}N4mpe)_4$ monolayer (**11**, Figure 8d) is 400 ± 100 s, 2 orders of magnitude larger than that of the **8** monolayer. This increase in τ_D suggests that stronger intermolecular interactions occur in the monolayer of **11** than in the monolayer of **8**. The τ_D value of the **11** monolayer, though, is still significantly smaller than those observed in peptoid monolayers that are collapse-competent, such as those composed of **9**.

The τ_D values obtained for the monolayers of **8**, **9**, and **11** correlate with the density of aromatic packing observed in recent crystal structures of cyclic dipeptoids, or *N*,*N*′-disubstituted diketopiperazines (DKPs), which serve as model compounds for understanding the packing within the nanosheet hydrophobic core.[19] Specifically, the lateral surface area of the N25dmpe monomer (27.8 Å^2 per N25dmpe-N25dmpe DKP molecule) is significantly less than that of the N2mpe monomer (41.5 Å per N2mpe-N2mpe DKP molecule) but is still larger than that of the N3mpe monomer (24.3 Å^2 per N3mpe-N3mpe DKP molecule). This suggests that N25dmpe monomers are able to pack at a higher density than for the N2mpe monomers but not as high as for the N3mpe monomers. Together, the τ_D values from the rheological measurements and lateral packing density from the DKP crystal structures suggest that the degree of aromatic packing is manifested in the monolayer stage of nanosheet assembly. Specifically, a greater degree of packing results in monolayers with strong intermolecular interactions so that the peptoid residence time in the monolayer is long enough to promote monolayer collapse.

Among peptoids in which the aromatic group is methyl-substituted at the ortho position (peptoids **8**, **11**, and **12**), monolayer collapse is recovered only when there is a second methyl group located at the para positions of the Npe aromatic ring (**12**, Figure 8e). Here, diffusion exchange again occurs at a rate that is too slow to access using the rheological experiments under study here. Although the rheological results suggest that **12** forms a solidlike monolayer with strong interchain interactions that promote nanosheet formation, the nanosheets formed from **12** degrade over the course of 1 week.[19] Results from the rheological studies can thus reveal only whether monolayer collapse and nanosheet formation occur but do not give an indication of the stability of nanosheets over extended periods of time. It is likely that substitution at the ortho position of the aromatic ring reduces peptoid chain flexibility such that these interchain interactions cannot be attained in the monolayer. Even though increased hydrophobic interactions due to the addition of a second substituent can overcome the limitation of chain inflexibility to promote monolayer collapse, having one methyl substituent at the ortho position still disrupts the formation of stable nanosheets.

DOI: 10.1021/acs.langmuir.6b02736
Langmuir XXXX, XXX, XXX−XXX

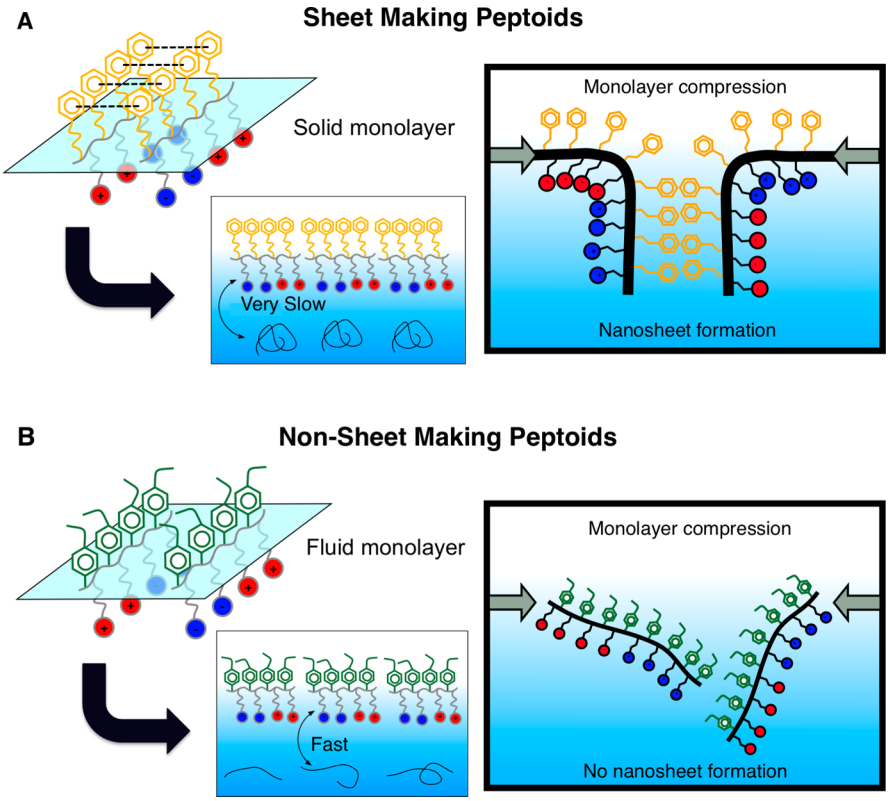

Figure 10. Cartoon depicting (A) the solidlike nature of peptoid monolayers that are capable of collapse into peptoid nanosheets upon monolayer compression and (B) the fluidlike nature of peptoid monolayers that do not collapse into peptoid nanosheets upon monolayer compression. For the solidlike monolayers, interchain interactions are relatively strong such that the peptoid residence time within in the monolayer is longer than 5000 s. For the fluidlike monolayers, interchain interactions are relatively weak such that the peptoid residence time within the monolayer is shorter than 500 s.

The final series of monolayers studied using surface dilational rheology consisted of those composed of peptoids with aliphatic hydrophobic monomers (Figure 9). Here, monolayers of both $(Nae\text{-}Ncp)_7\text{-}(Nce\text{-}Ncp)_7$ (**14**, Figure 9a) and $(Nae\text{-}Nch)_7\text{-}(Nce\text{-}Nch)_7$ (**15**, Figure 9b) exhibited τ_D values of 140 ± 10 and 27 ± 2 s, respectively. These values are indicative of fluidlike monolayers that do not collapse into nanosheets upon monolayer compression. This is consistent with our observation that peptoids **14** and **15** do not form nanosheets. However, branched, sheet-forming peptoid $(Nae\text{-}Nmbu)_7\text{-}(Nce\text{-}Nmbu)_7$ (**16**, Figure 9c) did not undergo peptoid desorption and readsorption on an accessible time scale, indicating a solidlike collapse-competent monolayer.

The surface dilational rheology results from the aliphatic peptoid series again demonstrate that peptoid flexibility is critical to forming a solidlike monolayer that is collapse-competent. For peptoids **14** and **15**, the cyclic hydrophobic substituents are branched directly adjacent to the peptoid backbone, thereby limiting flexibility. For peptoid **16**, nanosheets form despite the absence of $\pi-\pi$ interactions within the hydrophobic core. In this case, the side chain is also branched but at the β-carbon, thereby having less of a steric effect on the main chain. It is likely that the side-chain branching allows for strong-enough interchain interactions in the monolayer to form a solidlike monolayer capable of collapse into nanosheets.

CONCLUSIONS

When designing nanosheets with more elaborate chemical functionality, it is essential to develop an understanding of the mechanism by which self-assembly occurs and its tolerance to chemical modification. Through prior observation, it was apparent that the ability of a monolayer to adsorb to the air–water interface was necessary for nanosheet formation. However, we showed here that interfacial adsorption is not the only process that can limit the creation of a collapse-competent monolayer. In an effort to determine a set of design rules for peptoid sequences that form monolayers capable of collapse into nanosheets, we have extensively characterized a set of peptoid monolayers using surface dilation rheology. This analysis revealed a quantitative metric for predicting whether a peptoid monolayer will form nanosheets. Monolayer fluidity as represented by the residence time of the peptoid within the monolayer (τ_D) was related to the ability of a peptoid monolayer to collapse into bilayer nanosheets. All peptoid monolayers that formed nanosheets had τ_D values greater than 5000 s, indicating a slow rate of peptoid desorption and readsorption with the subphase during monolayer compression or expansion. These monolayers are solidlike, exhibiting strong interchain interactions that promote collapse upon monolayer compression. All peptoid monolayers that did not form nanosheets had τ_D values of less than 500 s, indicating a shorter peptoid residence time within the monolayer than seen for nanosheet-forming peptoids. The monolayers that did not form nanosheets were more fluidlike, exhibiting weaker interchain interactions. Upon compression, it is likely that individual chains desorb from the surface rather than a collective network of chains collapsing into nanosheets. The viscoelastic behavior of nonsheet-forming peptoids may in part be due to the relative inflexibility of the chains, preventing them from maximizing interchain interactions. These inflexible peptoids are ones in which the side-chain branch point is directly attached

DOI: 10.1021/acs.langmuir.6b02736
Langmuir XXXX, XXX, XXX–XXX

to the backbone nitrogen or when a substituent is located on the ortho position of the Npe aromatic ring. The differences in the peptoid monolayers that form nanosheets and those that do not are depicted in Figure 10.

Most importantly, small chemical modifications to the peptoid chain were manifested in the rheological behavior of the monolayer. This was seen for the main chain length series, in which an increase in length resulted in an increase in τ_D values; for the *N*-aryl monomer series, in which an increase in the ratio of Npe to Neph resulted in an increase in τ_D values; and for the methyl-substituted series, in which peptoids with dimethyl-substituted Npe aromatic rings had greater τ_D values when compared to the value for the peptoid with one methyl substituent at the ortho position. For all peptoids that did not form nanosheets, the τ_D values were used to determine when improvement to the sequence design had occurred. Such improvements cannot be assessed from qualitatively observing whether a specific peptoid was capable of forming nanosheets.

Our new understanding of the molecular-level interactions that lead to collapse-competent monolayers can be used in the design of peptoid sequences with increasingly complex chemical modifications. By relating small changes in the peptoid chemical structure to changes in the diffusion exchange rate, peptoids can be optimized to form a monolayer that is capable of collapse into nanosheets. Using surface dilational rheology measurements, peptoids can be rapidly screened for their ability to form nanosheets. This should be of great utility in the extension of the functionality of peptoid nanosheets into a variety of diverse applications.

■ ASSOCIATED CONTENT

Supporting Information

The Supporting Information is available free of charge on the ACS Publications website at DOI: 10.1021/acs.langmuir.6b02736.

Fitting parameters for all rheological data, the first few compression−expansion cycles shown in the isotherms for all monolayers, and the surface pressure vs area isotherm of the peptoid **6** monolayer at different adsorption times (PDF)

■ AUTHOR INFORMATION

Corresponding Author

*E-mail: rnzuckermann@lbl.gov.

Notes

The authors declare no competing financial interest.

■ ACKNOWLEDGMENTS

This project was funded by the Defense Threat Reduction Agency under contract no. DTRA10027-15875 and the DARPA Fold F(x) program. The work was conducted at the Molecular Foundry with support from the Advanced Light Source at Lawrence Berkeley National Laboratory, both of which are supported by the Office of Science, Office of Basic Energy Sciences, U.S. Department of Energy under contract no. DEAC02-05CH11231. The authors thank Rita Garcia for valuable assistance.

■ REFERENCES

(1) Butler, S. Z.; Hollen, S. M.; Cao, L.; Cui, Y.; Gupta, J. A.; Gutiérrez, H. R.; Heinz, T. F.; Hong, S. S.; Huang, J.; Ismach, A. F.; Johnston-Halperin, E.; Kuno, M.; Plashnitsa, V. V.; Robinson, R. D.; Ruoff, R. S.; Salahuddin, S.; Shan, J.; Shi, L.; Spencer, M. G.; Terrones, M.; Windl, W.; Goldberger, J. E. Progress, Challenges, and Opportunities in Two-Dimensional Materials Beyond Graphene. *ACS Nano* **2013**, *7*, 2898−2926.

(2) Govindaraju, T.; Avinash, M. B. Two-Dimensional Nanoarchitectonics: Organic and Hybrid Materials. *Nanoscale* **2012**, *4*, 6102−6117.

(3) Ariga, K.; Malgras, V.; Ji, Q.; Zakaria, M. B.; Yamauchi, Y. Coordination Nanoarchitectonics at Interfaces between Supramolecular and Materials Chemistry. *Coord. Chem. Rev.* **2016**, *320−321*, 139−152.

(4) Colson, J. W.; Dichtel, W. R. Rationally Synthesized Two-Dimensional Polymers. *Nat. Chem.* **2013**, *5*, 453−465.

(5) Moll, D.; Huber, C.; Schlegel, B.; Pum, D.; Sleytr, U. B.; Sara, M. S-Layer-Streptavidin Fusion Proteins as Template for Nanopatterned Molecular Arrays. *Proc. Natl. Acad. Sci. U. S. A.* **2002**, *99*, 14646−14651.

(6) Sakamoto, J.; van Heijst, J.; Lukin, O.; Schluter, A. D. Two-Dimensional Polymers: Just a Dream of Synthetic Chemists? *Angew. Chem., Int. Ed.* **2009**, *48*, 1030−1069.

(7) Zhuang, X.; Mai, Y.; Wu, D.; Zhang, F.; Feng, X. Two-Dimensional Soft Nanomaterials: A Fascinating World of Materials. *Adv. Mater.* **2015**, *27*, 403−427.

(8) Gangloff, N.; Ulbricht, J.; Lorson, T.; Schlaad, H.; Luxenhofer, R. Peptoids and Polypeptoids at the Frontier of Supra- and Macromolecular Engineering. *Chem. Rev.* **2016**, *116*, 1753−1802.

(9) Knight, A. S.; Zhou, E. Y.; Francis, M. B.; Zuckermann, R. N. Sequence Programmable Peptoid Polymers for Diverse Materials Applications. *Adv. Mater.* **2015**, *27*, 5665−5691.

(10) Mándity, I. M.; Fülöp, F. An Overview of Peptide and Peptoid Foldamers in Medicinal Chemistry. *Expert Opin. Drug Discovery* **2015**, *10*, 1163−1177.

(11) Yoo, B.; Shin, S. B. Y.; Huang, M. L.; Kirshenbaum, K. Peptoid Macrocycles: Making the Rounds with Peptidomimetic Oligomers. *Chem. - Eur. J.* **2010**, *16*, 5528−5537.

(12) Park, S.; Kwon, Y.-U. Facile Solid-Phase Parallel Synthesis of Linear and Cyclic Peptoids for Comparative Studies of Biological Activity. *ACS Comb. Sci.* **2015**, *17*, 196−201.

(13) Lee, J. H.; Meyer, A. M.; Lim, H.-S. A Simple Strategy for the Construction of Combinatorial Cyclic Peptoid Libraries. *Chem. Commun. (Cambridge, U. K.)* **2010**, *46*, 8615−8617.

(14) Holub, J. M.; Jang, H.; Kirshenbaum, K. Fit to Be Tied: Conformation-Directed Macrocyclization of Peptoid Foldamers. *Org. Lett.* **2007**, *9*, 3275−3278.

(15) Shah, N. H.; Butterfoss, G. L.; Nguyen, K.; Yoo, B.; Bonneau, R.; Rabenstein, D. L.; Kirshenbaum, K. Oligo(N-Aryl Glycines): A New Twist on Structured Peptoids. *J. Am. Chem. Soc.* **2008**, *130*, 16622−16632.

(16) Stringer, J. R.; Crapster, J. A.; Guzei, I. A.; Blackwell, H. E. Extraordinarily Robust Polyproline Type I Peptoid Helices Generated Via the Incorporation of Alpha-Chiral Aromatic N-1-Naphthylethyl Side Chains. *J. Am. Chem. Soc.* **2011**, *133*, 15559−15567.

(17) Robertson, E. J.; Battigelli, A.; Proulx, C.; Mannige, R. V.; Haxton, T. K.; Yun, L.; Whitelam, S.; Zuckermann, R. N. Design, Synthesis, Assembly, and Engineering of Peptoid Nanosheets. *Acc. Chem. Res.* **2016**, *49*, 379−389.

(18) Payamyar, P.; King, B. T.; Ottinger, H. C.; Schluter, A. D. Two-Dimensional Polymers: Concepts and Perspectives. *Chem. Commun.* **2016**, *52*, 18−34.

(19) Robertson, E. J.; Proulx, C.; Su, J. K.; Garcia, R. L.; Yoo, S.; Nehls, E. M.; Connolly, M. D.; Taravati, L.; Zuckermann, R. N. Molecular Engineering of the Peptoid Nanosheet Hydrophobic Core. **2016**, submitted for publication.

(20) Ruehs, P. A.; Affolter, C.; Windhab, E. J.; Fischer, P. Shear and Dilatational Linear and Nonlinear Subphase Controlled Interfacial Rheology of Beta-Lactoglobulin Fibrils and Their Derivatives. *J. Rheol.* **2013**, *57*, 1003−1022.

(21) Babak, V. G.; Desbrieres, J.; Tikhonov, V. E. Dynamic Surface Tension and Dilational Viscoelasticity of Adsorption Layers of a Hydrophobically Modified Chitosan. *Colloids Surf., A* **2005**, *255*, 119−130.

DOI: 10.1021/acs.langmuir.6b02736
Langmuir XXXX, XXX, XXX−XXX

(22) Diez-Pascual, A. M.; Monroy, F.; Ortega, F.; Rubio, R. G.; Miller, R.; Noskov, B. A. Adsorption of Water-Soluble Polymers with Surfactant Character. Dilational Viscoelasticity. *Langmuir* **2007**, *23*, 3802−3808.
(23) Freer, E. M.; Yim, K. S.; Fuller, G. G.; Radke, C. J. Shear and Dilatational Relaxation Mechanisms of Globular and Flexible Proteins at the Hexadecane/Water Interface. *Langmuir* **2004**, *20*, 10159−10167.
(24) Freer, E. M.; Yim, K. S.; Fuller, G. G.; Radke, C. J. Interfacial Rheology of Globular and Flexible Proteins at the Hexadecane/Water Interface: Comparison of Shear and Dilatation Deformation. *J. Phys. Chem. B* **2004**, *108*, 3835−3844.
(25) Noskov, B. A.; Bykov, A. G.; Grigoriev, D. O.; Lin, S. Y.; Loglio, G.; Miller, R. Dilational Visco-Elasticity of Polyelectrolyte/Surfactant Adsorption Layers at the Air/Water Interface: Poly(Vinyl Pyridinium Chloride) and Sodium Dodecylsulfate. *Colloids Surf., A* **2008**, *322*, 71−78.
(26) Miller, R.; Ferri, J. K.; Javadi, A.; Kraegel, J.; Mucic, N.; Wuestneck, R. Rheology of Interfacial Layers. *Colloid Polym. Sci.* **2010**, *288*, 937−950.
(27) Ravera, F.; Loglio, G.; Kovalchuk, V. I. Interfacial Dilational Rheology by Oscillating Bubble/Drop Methods. *Curr. Opin. Colloid Interface Sci.* **2010**, *15*, 217−228.
(28) Sanii, B.; Kudirka, R.; Cho, A.; Venkateswaran, N.; Olivier, G. K.; Olson, A. M.; Tran, H.; Harada, R. M.; Tan, L.; Zuckermann, R. N. Shaken, Not Stirred: Collapsing a Peptoid Monolayer to Produce Free-Floating, Stable Nanosheets. *J. Am. Chem. Soc.* **2011**, *133*, 20808−20815.
(29) Ravera, F.; Ferrari, M.; Santini, E.; Liggieri, L. Influence of Surface Processes on the Dilational Visco-Elasticity of Surfactant Solutions. *Adv. Colloid Interface Sci.* **2005**, *117*, 75−100.
(30) Sanii, B.; Haxton, T. K.; Olivier, G. K.; Cho, A.; Barton, B.; Proulx, C.; Whitelam, S.; Zuckermann, R. N. Structure-Determining Step in the Hierarchical Assembly of Peptoid Nanosheets. *ACS Nano* **2014**, *8*, 11674−11684.
(31) Ravera, F.; Ferrari, M.; Liggieri, L. Modelling of Dilational Visco-Elasticity of Adsorbed Layers with Multiple Kinetic Processes. *Colloids Surf., A* **2006**, *282-283*, 210−216.
(32) Monroy, F.; Kahn, J. G.; Langevin, D. Dilational Viscoelasticity of Surfactant Monolayers. *Colloids Surf., A* **1998**, *143*, 251−260.
(33) Vandentempel, M.; Lucassenreynders, E. H. Relaxation Processes at Fluid Interfaces. *Adv. Colloid Interface Sci.* **1983**, *18*, 281−301.
(34) Lucassen, J.; Van Den Tempel, M. Dynamic Measurements of Dilational Properties of a Liquid Interface. *Chem. Eng. Sci.* **1972**, *27*, 1283−1291.
(35) Langevin, D. Rheology of Adsorbed Surfactant Monolayers at Fluid Surfaces. *Annu. Rev. Fluid Mech.* **2014**, *46*, 47−65.
(36) Lucassen-Reynders, E. H.; Cagna, A.; Lucassen, J. Gibbs Elasticity, Surface Dilational Modulus and Diffusional Relaxation in Nonionic Surfactant Monolayers. *Colloids Surf., A* **2001**, *186*, 63−72.
(37) Mannige, R. V.; Haxton, T. K.; Proulx, C.; Robertson, E. J.; Battigelli, A.; Butterfoss, G. L.; Zuckermann, R. N.; Whitelam, S. Novel Secondary Structure of Biomimetic Polymers Enables Extended Two-Dimensional Assemblies. *Nature* **2015**, *526*, 415−420.

DOI: 10.1021/acs.langmuir.6b02736
Langmuir XXXX, XXX, XXX−XXX